Materials Research. 2021; 24(suppl. 1): e20210058
DOI: https://doi.org/10.1590/1980-5373-MR-2021-0058

CC BY

$SiO_xC_yH_z$-TiO_2 Nanocomposite Films Prepared by a Novel PECVD-Sputtering Process

Lucas Pires Gomes Oliveira[a*], Rafael Parra Ribeiro[a], José Roberto Ribeiro Bortoleto[a], Nilson Cristino Cruz[a], Elidiane Cipriano Rangel[a]

[a]Universidade Estadual Paulista (UNESP), Instituto de Ciência e Tecnologia de Sorocaba (ICTS), Laboratório de Plasmas Tecnológicos (LaPTec), Av. Três de Março, 511, 18087-180, Sorocaba, SP, Brasil.

Received: January 20, 2021; Revised: May 01, 2021; Accepted: June 16, 2021

Recently, there has been growing interest in the incorporation of particles in plasma deposited thin films to creation of multifunctional surfaces. In this work a new hybrid methodology based on the plasma enhanced chemical vapor deposition (PECVD) of hexamethyldisiloxane combined to the reactive sputtering of TiO_2 is proposed for the preparation of $SiO_xC_yH_z$-TiO_2 composite films. Specifically, the effect of the proportion of O_2 in the plasma environment on the morphology, chemical structure, elemental composition, wettability, thickness and surface roughness, of the films was studied. Agglomerates of TiO_2 (16-83 μm) were detected into the organosilicon matrix with the concentration of particulates growing with the percentage of oxygen in the feed. In general, there was elevation in the angle of contact of the surfaces as the oxygen supply increased. Interpretation is proposed in terms of the influence of the oxygen supply on the TiO_2 sputtering rate and in the oxidation of plasma species.

Keywords: *PECVD, HMDSO, Oxygen, Argon, Characterization.*

1. Introduction

The growing demand for materials of reduced dimensions and that perform specific functions has increased the interest in nanocomposite films[1,2]. These are defined as solids containing nano-dimensional phases with different properties from those found in the matrix. The great attention devoted to these materials in recent years is due to the fact that they provide results not achieved when macroscopic phases of each material are employed.

Amongst the different categories of nanocomposites, those involving particles of metallic oxides (SiO_2, Al_2O_3, CeO_2 and TiO_2) in silicon-based matrices generate coatings with chemical stability, high hardness, resistance to oxidation and to wear and with high refractive index and dielectric constant, with bactericidal and photo-electrochemical action[3].

There are reports in the literature showing that the immobilization of TiO_2 nanoparticles in Si-based films has demonstrated the potential for degradation of organic pollutants in gas and liquid phase[4]. In the area of biomaterials, SiO_2-TiO_2 nanostructures have been evaluated as alternatives to make the surface less receptive to biological cultures (bacteriostatic), or more detrimental to them (bactericides), a fact that avoids the inconveniences generated by the growth of biofilms on the implant surfaces[5,6]. There are also applications related to the protection of metal surfaces against corrosion. Estekhraji and Amiri[7], for example, produced nanostructured coatings SiO_2-TiO_2 and SiO_2-ZnO on aluminum by the sol-gel method. The addition of TiO_2 and ZnO nanoparticles resulted in a coating with enhanced hardness and corrosion resistance. Recently, a new type of cathodic protection technology, called photo-generated cathodic protection, has been investigated[8]. In this, electrons and vacancies (h^+) pairs are generated from the irradiation of the TiO_2 coating with ultraviolet light. The electrons created in this process are transferred from the semiconductor to the metallic substrate by the conduction band, increasing the negative potential of the metallic electrode in seawater and, thus, protection against corrosion. Vacancies, on the other hand, can promote, with low efficiency[9], the decomposition of water ($H_2O + 2h^+ \rightarrow 1/2\ O_2 + 2H^+$) instead of decomposing the semiconductor layer that is then preserved and can offer long-term protection for the metallic substrate. Based on this principle, Cheng et al.[8] applied, by the dip coating method, composite SiO_2-TiO_2 films on stainless steel. The analysis by electrochemical impedance spectroscopy showed less potential for corrosion for the samples analyzed with the incidence of UV light. The authors also suggest that the formation of Ti-O-Si bonds provides better photoelectrochemical properties than the Ti-O-Ti bond. Although the transfer of electrons to the substrate has a detrimental effect to the photocatalytic potential, it is beneficial to the protection of the metallic surface against corrosion and, once occurring in a moderate way, it may bring multifunctionality to the material.

Different methodologies are normally used to prepare SiO_2-TiO_2 nanocomposites, such as the sol-gel[10,11], hydrothermal[12] and plasma[13-15]. The sol-gel method is the most widespread for its simplicity, however the high consumption of solution[16] and the low adhesion of the films

*e-mail: luk.oliveira2013@gmail.com

to the substrates drive the development of alternatives. In this context, plasmas have been considered as clean, energetically, and economically viable method of producing nanocomposites with adjustable structures and controlled properties. Because it is a thermodynamical non-equilibrium methodology, alterations that are not viable by traditional chemical methods can be implemented in plasma. Thus, chemical, topographical and morphological modifications can be associated in one-step, dry, simple and viable treatments for large-scale applications. Although there are several studies on the production of TiO_2 films by sputtering and of SiO_2-TiO_2 nanocomposites by wet routes, no reports of the production of this composite by sputtering or by co-sputtering during PECVD were found.

Thus, the purpose of this work is to develop a one-step methodology for the synthesis of $SiO_xC_yH_x/TiO_2$ composite films, based on the plasma enhanced chemical vapor deposition, from the hexamethyldisiloxane compound, HMDSO, diluted with argon and oxygen, simultaneously to the sputtering of TiO_2. Specifically, it will be evaluated the effect of the proportion of oxygen and argon admitted to the deposition atmosphere on the deposition mechanisms and the properties of the resulting films.

2. Experimental

2.1. Plasma treatment

Films were collected in substrates of 1 cm x 2 cm prepared from glass (soda-lime-silica) and mirror-like aluminum (5052-H32). Prior to deposition, samples were chemically cleaned in an ultrasonic bath (Cristófoli) using the procedure described by Mancini et al.[17].

The films were deposited in a low-pressure plasma system, described in a previous work[18]. Figure 1 shows the schematic of the stainless-steel chamber with approximately 5.2×10^{-3} m^3 in volume where two circular, parallel electrodes (11.9 cm in diameter) are 5.0 cm apart. The system is evacuated by a rotary pump (Edwards E2M18) and the pressure monitored by a Pirani sensor (model APGX), located on the top flange of the reactor. The introduction of gases to the chamber is performed via a stainless-steel distribution system coupled to flexible polyamide tubes. The flow rate of the gases is controlled by needle valves (Edwards, model LV-10K). Liquid compounds, as hexamethyldisiloxane, are conditioned in an evaporation cell (100 ml Erlenmeyer) which is connected to a flange of the reactor via a needle valve. The gradient of pressure created by pumping induces the evaporation of the compound to the reactor when the valve is opened. A (RF) radiofrequency supply (Tokyo Hy-Power RF-300, 13.56 MHz, 0-300 W) is coupled, via an impedance matching circuit (Tokyo Hy-Power, model MB-300), to the lowermost electrode.

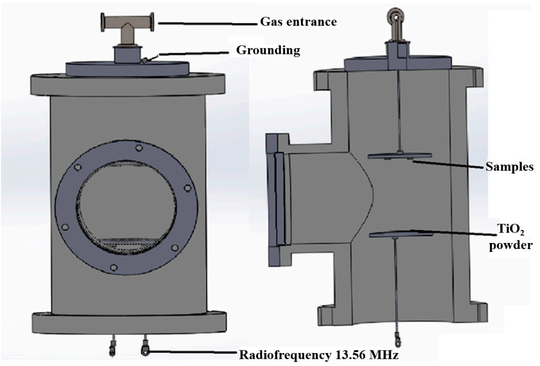

Figure 1. Schematic of the stainless-steel plasma chamber.

For the deposition procedures conducted here, clean substrates were attached to the upper electrode; 0.8 g of titanium dioxide powder (P25, Evonik) was spread on the center of the lower electrode and system was pumped down to the base pressure (2.0 Pa). To prevent TiO_2 dust from being carried to the vacuum system when pumping starts, a siphon-type connection between the reactor outlet and the pump inlet and/or filters for particulate material are recommended in this case.

The deposition atmosphere was then established by introduction of 2.0 Pa of the compounds participants of the process which were HMDSO (20%) and the dilution gases (80%), a mixture of Ar and O_2. In this way, the working pressure was of 4.0 Pa. The process was carried out without cooling the electrodes. Under similar conditions to those used here and using the same system, temperatures lower than 60°C are reported in the driven electrode (target)[19], but still lower values are expected for the grounded sample holder. The proportion of O_2 in the plasma was increased from 0 to 50% while that of Ar was decreased from 80 to 30% in order to keep the working pressure constant in all the experiments. The plasma was ignited by applying radiofrequency signal (13.56 MHz, 150 W) to the lower electrode were TiO_2 powder was spread. The upper electrode (sample holder) was grounded. In this configuration, it is induced low energy ion bombardment of the driven electrode, sputtering TiO_2 fragments to the PECVD process, produced from HMDSO. While argon proportion is decisive for sputtering it also plays a role on the activation of the HMDSO. Oxygen, on the other hand, chemically activates HMDSO and affects the overall chemistry of the PECVD process and of the resulting film. Thus, variation in the proportion of each dilution gas aims to find the synergy of their effects to provide the creation of the nanocomposites and allow the control of their characteristics. Deposition time was fixed in 1 hour for all the five depositions conducted here.

2.2. Characterization of the films

The chemical structure of the films was inspected by infrared spectroscopy in the IRRAS (Infrared Reflectance Absorbance Spectroscopy) mode with the aid of a Jasco FTIR 100-00 spectrometer. For each sample, 128 scans were recorded (400 to 4000 cm^{-1}) with resolution of 4 cm^{-1}, with the resulting spectrum being the arithmetic mean of these acquisitions. Samples were deposited on reflective substrates (polished aluminum) for this analysis. Elemental composition was determined by Energy Dispersive X-ray Spectroscopy (EDS) with the aid of a Dry SD Hyper detector, which presents a resolution of 129 to 133 eV on the Mn Kα emission line at 3000 cps and is coupled to a scanning electron microscope (JEOL JSM6010 LA). Spectra were

collected in 10 kV, on work distance to 10 mm for a spot size 70, amplified in 950x from samples metallized with a thin conductive layer, produced from the sputtering of an Au/Pd target.

The surface thermodynamical properties of the samples were investigated in a Ramé-Hart 100-00 goniometer, using samples deposited on glass slides. Drops of 2.0 µl of deionized water and diiodomethane were deposited in three different positions of each sample, and the contact angle measured at room temperature and under controlled humidity conditions.

The layer thickness was determined by profilometry using glass samples whose surfaces were only partially subjected to the deposition process. For that, a part of the substrate area was protected with a mask (Kapton® adhesive tape (3M)) and the system submitted to the deposition process. After completion and removal of the mask, a step was created between the protected from and exposed to plasma areas. The step height, which represents the thickness of the film, was measured by profiles acquired from three different positions. For the acquisition of each profile, the tip was scanned 2000 µm along the step under load of 3.0 mg. Five measurements were made in each profile providing 15 values of thickness per sample. For the roughness analysis, the same procedures were adopted, but using glass samples without the step, that is, those in which the film was uniformly deposited.

The surface microstructure of the samples was inspected by scanning electron (SEM) and atomic force (AFM) microscopies. Secondary electron micrographs were recorded from samples prepared on polished aluminum in a JEOL JSM 6010LM equipment. To avoid charging, the samples metallized with Au-Pd (60 mA and 60 seconds) were used in these analyses. The micrographs were acquired with magnifications of 2500 and 5000x, beam energy of 3.0 kV and spot size of 30. Topographic profiles of 5 µm x 5 µm were acquired by AFM in a Park-systems XE-100 equipment, in the non-contact mode, employing a silicon tip of 5 nm nominal radius.

3. Results and Discussion

The thickness of the films is presented in Figure 2 as a function of the proportion of oxygen in the deposition atmosphere, O_2%, determined from the samples deposited on glass slides. In general, films hundreds of nanometers thick were obtained. As the deposition time was kept constant (60 min), the deposition rate follows exactly the same trend as the thickness. A general reduction in layer thickness and deposition rate are observed when oxygen is incorporated to plasma. There is a steep drop when low proportions of O_2 are used (up to 20%) while a new growing trend is observed for $O_2\% > 20\%$. The same trend was observed in the work of Duarte, Massi and Sobrinho[20]. Considering that the highest (0% O_2) and the lowest (20% O_2) deposition rates were 6.6 and 3.1 nm/min, respectively, it is noticed that O_2% affects only subtly the deposition rate.

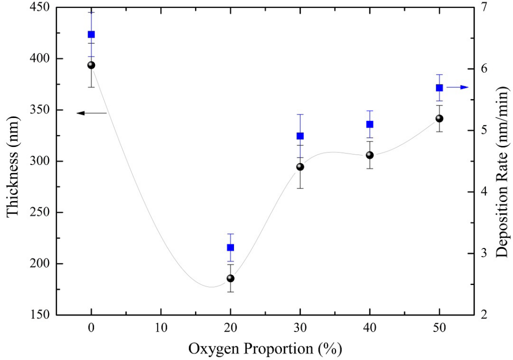

Figure 2. Film thickness and deposition rate as a function of the proportion of O_2 admitted in the plasma dilution.

To understand this behavior, one must consider firstly that Ar acts as a plasma activator. The presence of this element in moderate proportions increases the average energy and/or average density of the plasma species[20], and thus the proportion of reactive species. Besides its effect on the direct and indirect activation of HMDSO molecules, generating fragments that are the precursors for film formation, Ar promotes ion bombardment of the driven electrode where TiO_2 is placed, emitting species of this compound to the plasma. So, when the dilution atmosphere is composed only of Ar (0% O_2), the plasma activity is high as well as the sputtering effectiveness. When 20% of O_2 is admitted, there is a sudden reduction in the deposition rate. Lin et al.[21], published a study in which the mean temperature of the plasma electrons generated from mixtures of argon and oxygen was analyzed using optical emission spectroscopy (OES). The results showed that the average electron temperature decreases with an increase in the oxygen flow above a certain value. This tendency, also observed by Safeen et al.[22], is attributed to the absorption of electrons by oxygen molecules, generating negative species, such as O^- e O_2^-[21]. Besides its effect on electron density, the sticking coefficient of oxygen species on metals is around 1. In other words, oxygen active groups are lost from the plasma atmosphere, also contributing to the overall reduction in deposition rate and layer thickness with respect to that observed with pure argon dilution. Owing to such phenomena, the chemical effect of oxygen on the HMDSO activation does not overcome that of reduction in the plasma activity, caused by the lowering in the Ar content. A higher proportion of O_2 is necessary to enhance the activation of the precursor compound and to elevate the deposition rate, explaining the rising trend in deposition rate with increasing O_2%. Nevertheless, the abundance of reactive species from oxygen brings further consequences: it affects the sputtering process and the film etching. As in oxygen plasmas, O^+ and O^{2+} are generated, it is postulated they also contribute to ejection of fragments of TiO_2 by ion bombardment. However, the probability of oxygen ions to stick on the target is much higher than that of removing material by sputtering. Oxygen abundance and film deposition process also favors the target poisoning, reducing the sputtering yield of TiO_2. Because of these facts, and of the low energy ion bombardment provided in the present configuration of the plasma system, deposition kinetics is dominated by HMDSO fragmentation, with titanium dioxide contributing as a secondary phase for film growth. Then, the lower deposition rates when O_2 is present is ascribed to the oxygen effect on the plasma activity, provoke by loss of electrons, loss of reactive species and by reduction of the

Ar content, as well as on the removal of material from the film (etching). The effect of the O_2% on TiO_2 sputtering rate thus affects the incorporation of the secondary phase in the resulting film. Finally, it is considered that TiO_2 deposition mechanism approaches that propose by Berg and Nyberg[23].

The average roughness of the samples deposited on glass slides is shown in Figure 3. The roughness of the as-received glass is around 150 nm (horizontal line). An increment of this value is observed when the oxygen proportion is increased beyond 20% while a reduction is evidenced when O_2% is lowered (< 20%). To understand these results, micrographs obtained from samples prepared on Al are presented in Figure 4.

It is evident in these micrographs that the aluminum substrate has imperfections inherent to the manufacturing process, which are totally or partially covered by the deposition of the film. The film alters the substrate's morphology regardless of the employed deposition condition. For low proportions of O_2 (< 20%) the surface is smoothened by the growth of a uniform film, which is consistent with the roughness result shown in Figure 3. The condition that promoted the highest deposition rate also resulted in one of the smoothest films (0% O_2). In some cases, even after exposure to plasma, the deeper scratches of the substrate are still evident on the surface, a fact consistent with the layer thicknesses. In addition to these, irregular clusters with a porous morphology appear, suggesting the presence of a uniform covering with particulates linked to it. With increasing O_2%, there is an elevation in the concentration of particulate material present on the surface, which can be pointed out as the factor responsible for the roughness rise in Figure 3. The same effect has already been observed in the work of Darriba and collaborators[19]. The roughness of oxides, in general, decreases with the oxygen content due to the reduction in the deposition rate and the enhancement in exothermic processes taking place on film surface during the growth. But in the present case, deposition rate increases with increasing O_2%, once the process is not a conventional sputtering deposition and is dominated by HMDSO activation.

As can be noticed, the results of surface morphology consistently explain those of roughness although both have

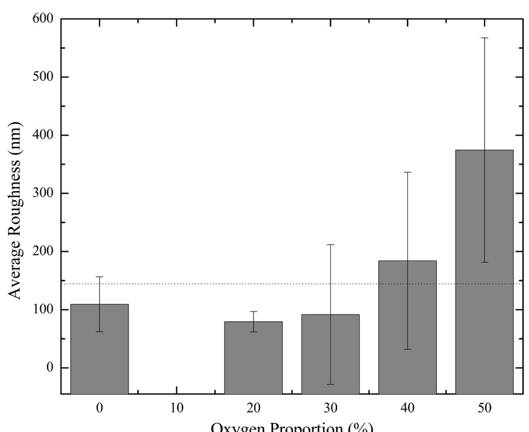

Figure 3. Film roughness as a function of the proportion of O_2 admitted in the plasma dilution.

been obtained from samples prepared on different substrates (glass and Al). This fact suggests that similar films may be obtained on substrates with different chemical natures (metallic-glassy) and electrical properties (dielectric-conductive), as already verified in previous works[24,25].

Figure 5 shows 5 μm x 5 μm topographic profiles acquired from the film matrix, that is, outside the region of micrometric particles, for samples deposited on polished aluminum. In this scale it is observed that film does not completely hide the defects of the substrate. However, in all cases it is identified the presence of a film with granular structure typically observed in films deposited from HMDSO by PECVD[24-26]. Variations in O_2% produce a gradual change in the film's topography which is smoothened for oxygen additions of up to 40%, but becomes rougher when 50% of O_2 is admitted. Besides affecting the morphology of the film, O_2% also influences the characteristics of the granulates incorporated in the structure, which appear as lighter points in the images. Firstly, the concentration of particulates growths with increasing O_2%. In addition, they appear more integrated to the structure when 20% of O_2 is used to dilute the plasma. More uniform (rounded) particulates are observed in depositions conducted with 0% and 40% of O_2 in the plasma while the larger ones are observed for 30% of O_2. Although at different scales, these results show good agreement with the scanning electron micrographs of the samples and may have influence on the properties of the films in specific applications.

The infrared spectra (IRRAS) of the samples deposited on polished aluminum are depicted in Figure 6. The spectra show characteristic groups of the organosilicon structure, namely, Si-O-Si (803 and 1042 and cm^{-1})[27,28], Si-$(CH_3)_x$ (1251 cm^{-1})[29], CH_3 (2939 and 2954 cm^{-1})[30]. Interestingly, the band at around 1260 cm^{-1} disappears from the spectra of the films deposited with higher oxygen proportions (> 20%) while another one, attributed to Si-O-C groups, emerges at 1240 cm^{-1}, indicating the transformation of the organosilicon film into a silicon oxycarbide.

Hydrogen removal from methyl groups by active oxygen of the plasma, process enhanced with the growth of O_2%, explains the formation mechanism of this network. The de-hydrogenated structure has Si-O-C and Si-C-O groups as well as Si-O-Si characterizing it as a hybrid between silica and silicon oxycarbide. The concentration of HMDSO fragments in the plasma grows with increasing O_2 proportion beyond 20%, explaining the rise in the deposition rate and thickness of the films (Figure 2), but without changing chemical nature of the material. On the other hand, structural changes related to the incorporation of TiO_2 groups are detected between 500-1500 cm^{-1}. From the TiO_2 (P25) spectrum in the same figure, the broadband as well as the shoulders on it, represent contributions ascribed to titanium dioxide, namely 492 (Ti-O-Ti)[24], 667 (Ti-OH) and 750 cm^{-1} (TiO_2 network vibrations)[31]. In general, the elevation in O_2% promotes removal of organic groups (CH_3) from the organosilicon structure, favoring the creation of an intermediate network between the SiO_2 and the Si-O-C, besides the TiO_2 incorporation. The vibration of Si-O-Ti groups is expected to provide contributions in 667 cm^{-1} and between 993-998 cm^{-1}. Thus, the bands observed in these

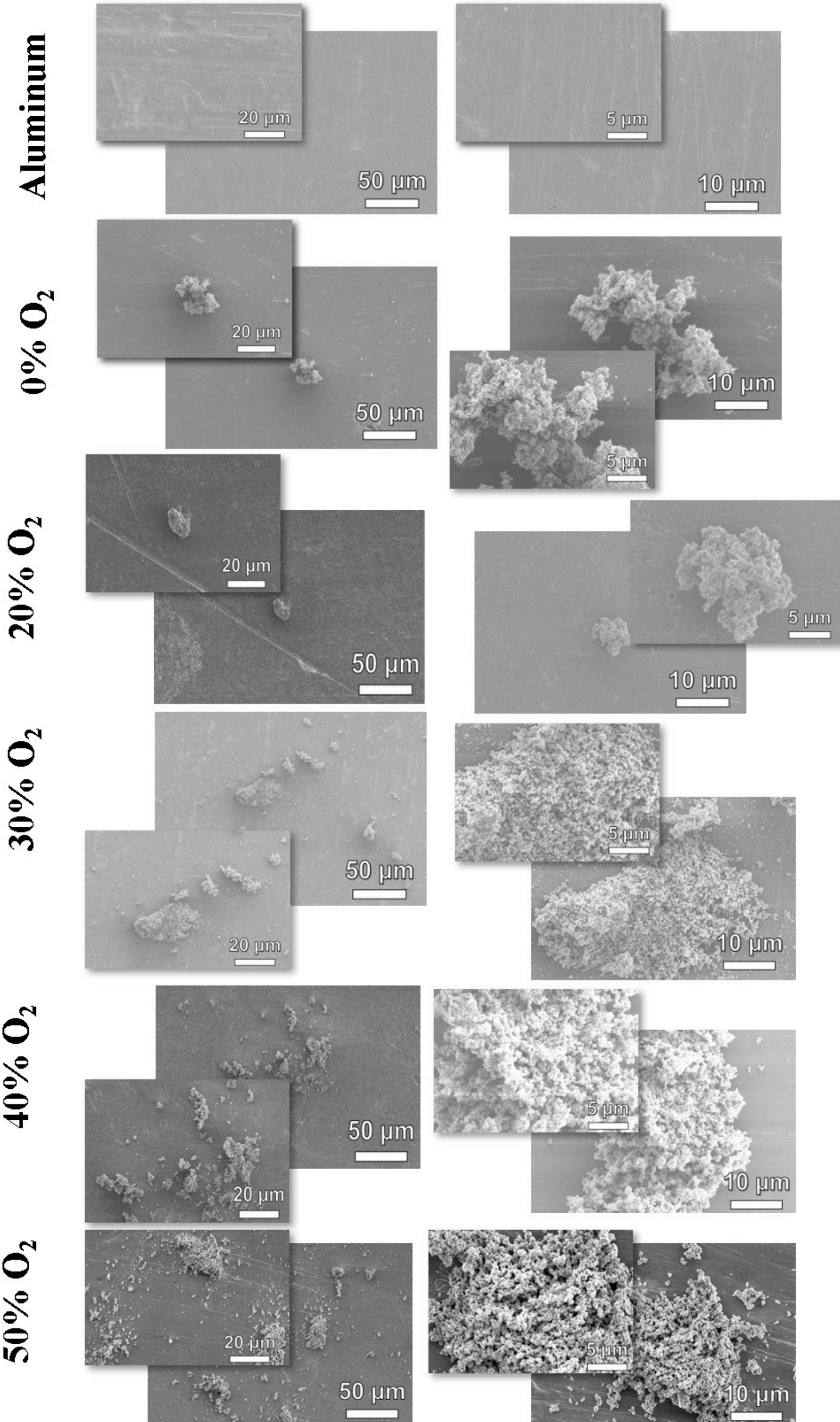

Figure 4. Secondary electron micrographs of samples deposited on aluminum in plasmas containing different proportions of oxygen. The micrograph of the Al substrate is also presented.

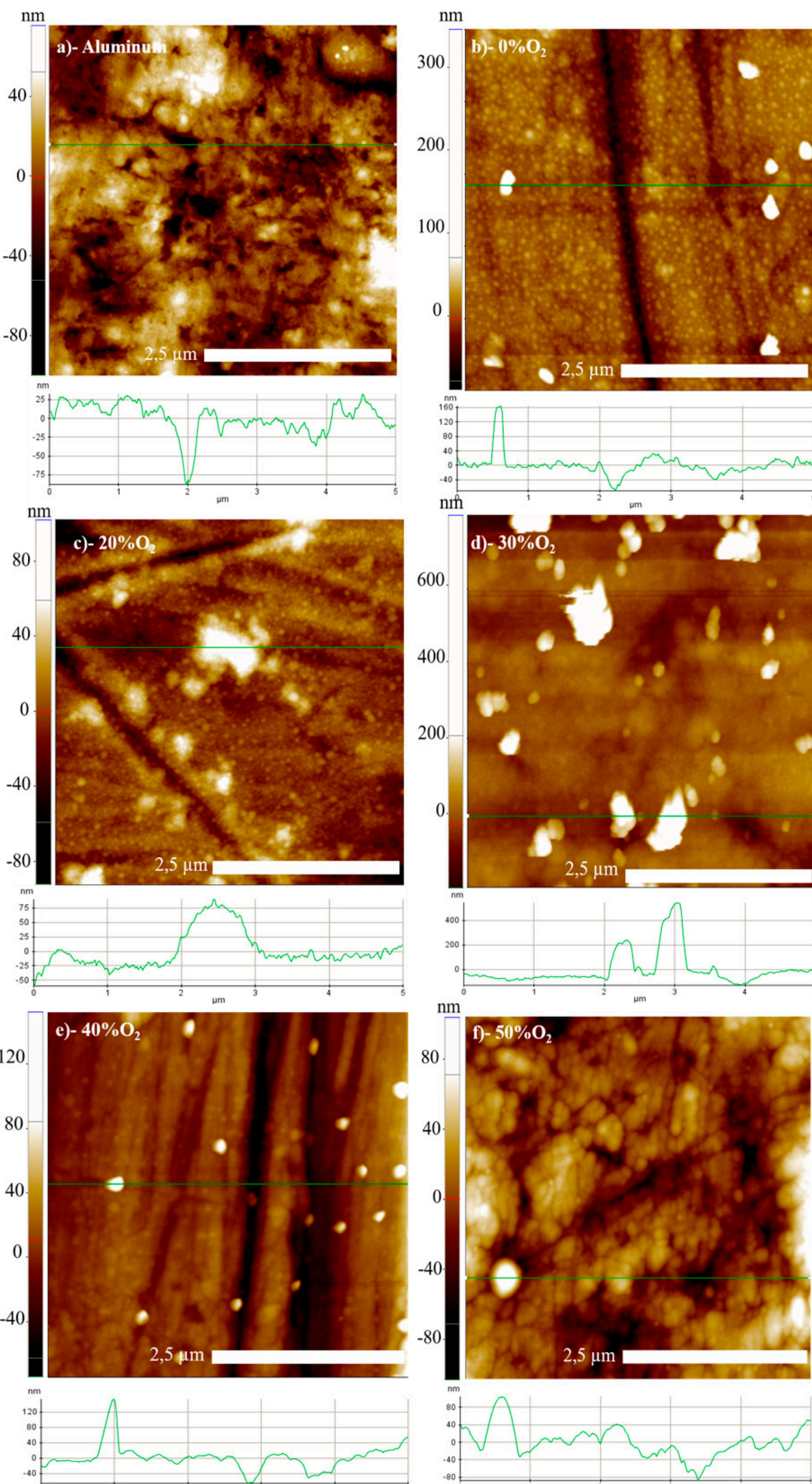

Figure 5. Topographic profiles of samples deposited on polished aluminum plates in plasmas containing different proportions of oxygen.

regions for the spectra of films deposited with the higher O_2%, may also have the contribution of functional Si-O-Ti.

The atomic proportions of the elements derived from the EDS spectra of the samples and the substrate (polished aluminum) are presented in Figure 7a. Although the elements of the substrate (Al, Mg) are detected in all samples, when they are disregarded in the calculations, Figure 7b, result in an upward trend in the titanium content when $O_2\% > 20\%$.

That is, the sputtering promoted by Ar is not the exclusive mechanism for the incorporation of TiO_2. Chemical reactions catalyzed by oxygen seems to play a role in this process. Furthermore, films that presented the highest proportion of Ti also presented higher proportions of Si and O. According to the chemical structure results, the higher the concentration of oxygen present in the plasma the faster the removal of carbon. However, the creation of a layer of Ti oxide particles spread on the surface, by itself affects the results obtained from deeper layers. Finally, the results of elementary composition corroborate the proposal of incorporating Ti on the surface of a Si-based film.

The compositional maps of the samples were registered by EDS and are shown in Figure 8. By the chemical results, it is observed a continuous Si-based structure with the arising of agglomerates composed of Ti and O. Carbon is hardly detected in the particulates, however, Ti is verified to be uniformly spread on the film matrix, corroborating the proposal that this element takes part in the PECVD reactions and thus is incorporated in the film.

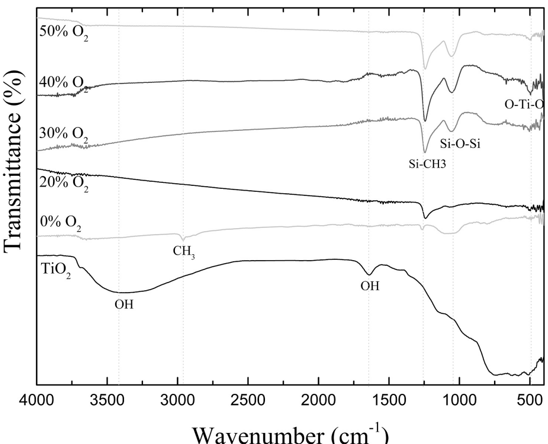

Figure 6. Transmission infrared spectra of the films deposited with different percentages of oxygen in the feed. The spectrum of TiO_2 (P25 Evonik) is also shown.

The contact angle of the films, θ, is depicted in Figure 9 as a function of the oxygen proportion in the plasma. Data were acquired using deionized water and diiodomethane. The corresponding values for the uncoated substrate (glass) are also presented. For the non-polar compound, the contact angle is reduced with enhancing O_2% up to 30%, rising afterwards. The most receptive surface to non-polar fluids was obtained with 30% of O_2 dilution. Considering the results for water, a hydrophobic surface is originated from the depositions without O_2 in the plasma (0% O_2), what is in good agreement with the predominantly organosilicon nature of this sample. The incorporation of Ti does not substantially affect the wettability of the organosilicon, possibly due to its reduced proportion (Figure 8). When O_2 is incorporated (20%) and the resulting structure is a silicon oxycarbide, there is a drop in θ reaching about (35°). There is growth trend in θ with further increasing the O_2 proportion in the plasma, regime in which the transition to a hybrid structure of SiO_2 with Si-O-C inclusions was identified. However, as wettability is a property essentially dependent on the first atomic layers of the material, the increase in θ with O_2% is attributed to the greater incorporation of TiO_2 particulates on these surfaces. Studies in the literature report values between 80-90° for the contact angle of the TiO_2 used here (P25)[1,2]. Comparing the trends obtained in contact angle and roughness with increasing O_2%, there are no direct correlations among them, indicating that the main factor responsible for the growth in θ with O_2% is, in fact, due to chemical changes promoted on the surface.

The group of results presented here, points to creation of a composite structure in which titanium oxides particulates are incorporated in a Si-based film, by a single step-plasma methodology. Further studies will be conducted to verify the effect of this incorporation on the photocatalytic activity, microbial effect and corrosion resistance of the samples.

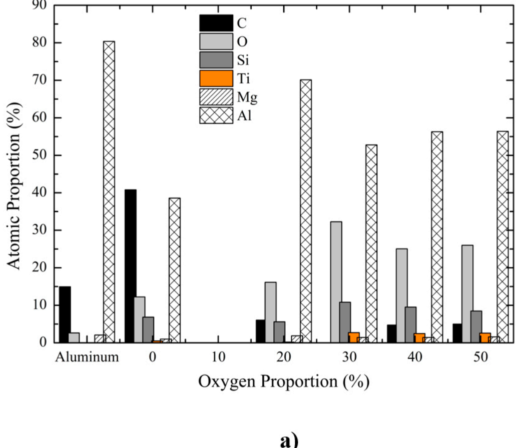

a)

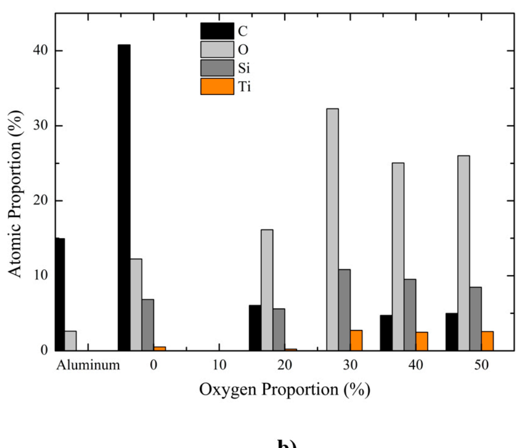

b)

Figure 7. (a) Atomic proportion originally obtained from samples deposited with different proportions of O_2 in the plasma. (b) Atomic percentage of the elements found in the samples treated with different proportions of O_2 in the plasma, but without considering the elements of the substrate. In both graphs the correspondent results for the Al substrate are presented.

Figure 8. Compositional maps of samples prepared in plasmas containing different proportions of O_2.

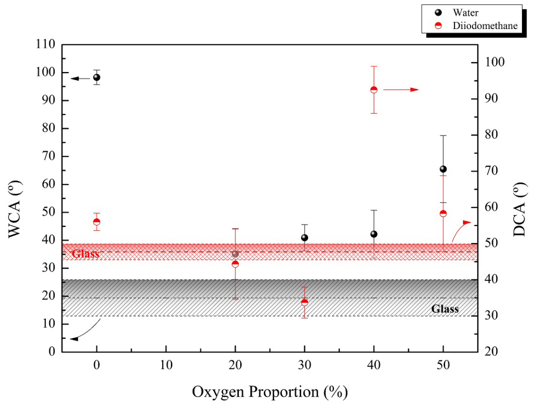

Figure 9. Contact angle as a function of the percentage of oxygen in the feed for distilled water (right axis) and diiodomethane (left axis). Contact angles of the glass substrate are also given by the dashed areas.

4. Conclusions

In the methodology proposed here the proportion of oxygen in the plasma dilution affects the deposition kinetics as well as the film properties.

The kinetics alterations are induced once oxygen contributes to removal of organic groups from the HMDSO fragments, transforming the organosilicon film into a silicon oxycarbide and silicon oxide mixed structure. Oxygen also affects the density of electrons, the target poisoning process, the sputtering yield, the fragmentation of HMDSO and the etching of the grown film. Owing to a combination of such effects, deposition rate and Ti incorporation are altered. The concentration, size and form of the particulate phase as well as the surface microstructure and the roughness of the composite films are all affected by oxygen admission in the plasma. Surface wettability by water can be shifted from hydrophobic to hydrophilic by means of chemical and structural changes induced by variations in the proportions of the dilution gases. Film deposition is dominated by the PECVD of HMDSO, whereas TiO_2 deposition is a secondary process. These different contributions of the PECVD and sputtering allowed the creation of a silicon-based structure containing TiO_2 particulate material.

Therefore, considering the association of the results presented here, it is demonstrated the possibility of preparing $SiO_xC_yH_z/TiO_2$ composite films using the one-step methodology that combines the PECVD of the HMDSO and the sputtering of TiO_2. It was also demonstrated the possibility of adjusting the composites properties by controlling the proportion of O_2 and Ar in the plasma.

5. Acknowledgments

Authors would like to thank the financial support of the Brazilian agencies *Fundação de Apoio à Pesquisa do Estado de São Paulo* - FAPESP (Process 2017/21034-1) and *Coordenação de Aperfeiçoamento de Pessoal de Nível Superior* – CAPES (Processes 1754231/2017 and 1560670/2015).

6. References

1. Patel MH, Chaudhuri TK, Patel VK, Shripathi T, Deshpande U, Lalla NP. Dip-coated PbS/PVP nanocomposite films with tunable band gap. RSC Advances. 2017;7(8):4422-9.
2. Kim TI, Kwon B, Yoon J, Park IJ, Bang GS, Park YK, et al. Antibacterial activities of graphene oxide-molybdenum disulfide nanocomposite films. ACS Appl Mater Interfaces. 2017;9(9):7908-17.
3. Ramaprakash M, Sreedhar G, Mohan S, Panda SK. Corrosion protection studies of CeO2–TiO2 nanocomposite coatings on mild steel. Transactions of the Institute of Metal Finishing. 2016;94(5):254-8.
4. Suligoj A, Lavrenciic Stangar U, Ristić A, Mazaj M, Verhovsek D, Tusar NN. TiO2 – SiO2 films from organic-free colloidal TiO2 anatase nanoparticles as photocatalyst for removal of volatile organic compounds from indoor air. Appl Catal B. 2016;184:119-31.
5. Nithyadevi P, Rathish RJ, Bama JS, Rajendran S, Joany RM, Pandiarajan M, et al. Inhibition of corrosion of mild steel in well water by TiO2 nanoparticles and an aqueous extract of May flower. Nanosystems: Physics, Chemistry, Mathematics. 2016;7(4):711-23.
6. Costa ACFM, Vilar MA, Lira HL, Kiminami RHGA, Gama L. Síntese e caracterização de nanopartículas de TiO2. Ceramica. 2006;52(324):255-9.
7. Estekhraji SAZ, Amiri S. Synthesis and characterization of anti-fungus, anti-corrosion and self-cleaning hybrid nanocomposite coatings based on sol–gel process. J Inorg Organomet Polym Mater. 2017;27(4):883-91.
8. Cheng W, Li C, Ma X, Yu L, Liu G. Effect of SiO2-doping on photogenerated cathodic protection of nano-TiO2 films on 304 stainless steel. Mater Des. 2017;126(April):155-61.
9. Fujishima A, Zhang X, Tryk DA. TiO2 photocatalysis and related surface phenomena. Surf Sci Rep. 2008;63(12):515-82.
10. Cheng Z, Cheng K, Weng W. SiO2/TiO2 nanocomposite films on polystyrene for light-induced cell detachment application. ACS Appl Mater Interfaces. 2017;9(3):2130-7.
11. Yaseen M, Shah Z, Veses RC, Dias SLP, Lima ECS, dos Reis G, et al. Photocatalytic studies of Tio2/Sio2 nanocomposite xerogels. J Anal Bioanal Tech. 2017;8(1):8-11.
12. Thi T, Quyen B, Thi N, Chi X, Thien DVH, Le B, et al. Synthesis of SiO 2/TiO 2 nanocomposites under supporting of microwave with SiO 2 from RHA and its catalytic activity. Int J Sci Eng Technol. 2017;6(3):108-12.
13. Gandhiraman RP, Daniels S, Cameron DC. A comparative study of characteristics of SiOx CyHz, TiOx and SiO-TiO oxide-based biocompatible coatings. Plasma Process Polym. 2007;4(Suppl 1):369-73.
14. Fanelli F, Fracassi F. Aerosol-assisted atmospheric pressure cold plasma deposition of organic-inorganic nanocomposite coatings. Plasma Chem Plasma Process. 2014;34(3):473-87.
15. Zhao Z, Sun J, Xing S, Liu D, Zhang G, Bai L, et al. Enhanced Raman scattering and photocatalytic activity of TiO2 films with embedded Ag nanoparticles deposited by magnetron sputtering. J Alloys Compd. 2016;679:88-93.
16. Drew K, Girishkumar G, Vinodgopal K, Kamat PV. Boosting fuel cell performance with a semiconductor photocatalyst: TiO 2/Pt-Ru hybrid catalyst for methanol oxidation. J Phys Chem B. 2005;109(24):11851-7.
17. Mancini SD, Nogueira AR, Rangel EC, Da Cruz NC. Solid-state hydrolysis of postconsumer polyethylene terephthalate after plasma treatment. J Appl Polym Sci. 2013;127(3):1989-96.
18. Souza JGS, Bertolini M, Costa RC, Cordeiro JM, Nagay BE, De Almeida AB, et al. Targeting Pathogenic Biofilms: Newly Developed Superhydrophobic Coating Favors a Host-Compatible Microbial Profile on the Titanium Surface. ACS Appl Mater Interfaces. 2020;12(9):10118-29.
19. Battaglin FAD, Hosokawa RS, da Cruz NC, Caseli L, Rangel EC, da Silva TF, et al. Innovative low temperature plasma approach for deposition of alumina films. Mater Res. 2014;17(6):1410-9.
20. Duarte DA, Massi M, Da Silva Sobrinho AS. Comparison between conventional and hollow cathode magnetron sputtering systems on the growing of titanium dioxide thin films: A correlation between the gas discharge and film formation. EPJ Applied Physics. 2011;54(2):1-7.
21. Lin Z, Li SJ, Sun F, Ba DC, Li XC. Surface characteristics of a dental implant modified by low energy oxygen ion implantation. Surf Coat Tech. 2019;365:208-13.
22. Safeen K, Micheli V, Bartali R, Gottardi G, Laidani N. Low temperature growth study of nano-crystalline TiO2 thin films deposited by RF sputtering. J Phys D Appl Phys. 2015;48(29)
23. Berg S, Nyberg T. Fundamental understanding and modeling of reactive sputtering processes. Thin Solid Films. 2005;476(2):215-30.
24. Rangel RCC, Cruz NC, Milella A, Fracassi F, Rangel EC. Barrier and mechanical properties of carbon steel coated with SiOx/SiOxCyHz gradual films prepared by PECVD. Surf Coat Tech. 2019;378:124996.
25. Santos NM, Gonçalves TM, de Amorim J, Freire CMA, Bortoleto JRR, Durrant SF, et al. Effect of the plasma excitation power on the properties of SiOxCyHz films deposited on AISI 304 steel. Surf Coat Tech. 2017;311:127-37.
26. Vendemiatti C, Hosokawa RS, Rangel RCC, Bortoleto JRR, Cruz NC, Rangel EC. Wettability and surface microstructure of polyamide 6 coated with SiOXCYHZ films. Surf Coat Tech. 2015;275:32-40.
27. Jin SB, Choi YS, Choi IS, Han JG. Surface energy modification of SiOxCyHz film using PECVD by controlling the plasma processes for OMCTS (Si 4O4C8H24) precursor. Thin Solid Films. 2011;519(20):6763-8.
28. Lee JH, Pham Thuy TT, Kim YS, Lim JT, Kyung SJ, Yeom GY. Characteristics of SiO2-Like thin film deposited by atmospheric-pressure PECVD using HMDS/O2/Ar. J Electrochem Soc. 2008;155(3):D163.
29. Lovascio S. Cold plasma deposition of organosilicon films with different monomers in a dielectric-barrier discharge [thesis]. Paris: Université Pierre et Marie Curie; 2010.
30. Cai H, Mu W, Liu W, Zhang X, Deng Y. Sol-gel synthesis highly porous titanium dioxide microspheres with cellulose nanofibrils-based aerogel templates. Inorg Chem Commun. 2015;51:71-4.
31. Farmer VC. Infrared spectra of minerals. England: Mineralogical Society of Great Britain and Ireland; 1974.